ADVANCED SCIENCE NEWS
www.advancedsciencenews.com

Compound Homojunction:Heterojunction Reduces Bulk and Interface Recombination in ZnO Photoanodes for Water Splitting

*Ning Wang, Min Liu, Hairen Tan, Junhui Liang, Qixing Zhang, Changchun Wei, Ying Zhao, Edward H. Sargent, and Xiaodan Zhang**

The photoelectrochemical (PEC) splitting of water utilizing sunlight to produce hydrogen has attracted much attention in light of its potential to store solar energy in a convenient way.[1–4] Among materials for PEC applications, ZnO has been widely investigated as a photoanode because of its favorable band-edge position, high photocatalytic activity, and high electron mobility.[5–9] However, the PEC performance of ZnO photoelectrodes is strongly limited by the bulk and interface recombination of charge carriers,[10–12] as depicted in **Figure 1**a. Charge recombination arises from poor conductivity, low hole mobility (1–15 $cm^2\ V^{-1}\ s^{-1}$ at 300 K), and sluggish oxygen evolution reaction kinetics.[13] Attempts to improve charge separation and transfer have been made, such as through the use of heterojunctions,[14–16] multi-dimensional nanostructures,[17,18] and oxygen evolution catalysts.[19] However, it is still challenging to simultaneously reduce the bulk and interface recombination losses.

The use of a heterojunction is a well-established concept in semiconductor devices to enhance charge separation and charge transport. Unfortunately, even mildly suboptimal growth conditions can produce a large density of defects at the interface. These can serve as deep traps that enhance, rather than mitigate, recombination.[20,21]

Dr. N. Wang, Dr. J. H. Liang, Dr. Q. X. Zhang, Prof. C. C. Wei, Prof. Y. Zhao, Prof. X. D. Zhang
Institute of Photoelectronic thin Film Devices and Technology of Nankai University
Key Laboratory of Photoelectronic Thin Film Devices and Technology
Collaborative Innovation Center of Chemical Science and Engineering
Nankai University
Tianjin 300071, P. R. China
E-mail: xdzhang@nankai.edu.cn
Dr. M. Liu, Dr. H. R. Tan, Prof. E. H. Sargent
Department of Electrical and Computer Engineering
University of Toronto
35 St George Street, Toronto, Ontario M5S 1A4, Canada
Dr. H. R. Tan
Photovoltaic Materials and Devices Laboratory
Delft University of Technology
2628CD Delft, The Netherlands

DOI: 10.1002/smll.201603527

We posited that introducing a homojunction to distribute a built-in electric field in the ZnO bulk could produce a desirable gradient in the carrier concentration; this could have the benefit of proving carrier separation away from the sites most prone to recombination. Specifically, we developed herein an n^+–n homojunction in which the gradient in carrier concentration produces a spatial variation in the Fermi level,[22] providing a built-in electronic field that enhances the bulk charge separation and transfer. Using this concept, we demonstrate ZnO n^+–n multi-layer thin-film devices (shown in Figure 1b) to enhance the PEC performance.

Oxygen vacancies in metal oxides typically act as electron donors, thereby enhancing electrical conductivity and charge transport.[23] We therefore introduced oxygen vacancies at the ZnO surface using Se-doping, all with the goal of suppressing interfacial recombination as oxygen vacancies will accept electrons and retain them for an extended transient period.[24] As illustrated in Figure 1b and c, the catalyst-free ZnOSe/ZnO/BZO multi-layer (BZO = boron-doped zinc oxide) is designed not only to suppress bulk recombination via the n^+–n homojunction, but also to reduce interfacial recombination via the introduction of surface oxygen vacancy defects.

X-ray diffraction (XRD) and scanning electron microscopy (SEM) analysis allowed us to investigate how B and Se doping affects the crystal structure and surface morphology of the ZnO photoanode. As shown in **Figure 2**, the doping with B and Se atoms does not affect the crystal structure nor the surface morphology of the ZnO. A preferred growth orientation along the (110) peak, and a sharp pyramidal shape, were observed for ZnO, ZnO/BZO-homojunction, and ZnOSe/ZnO/BZO photoanodes. However, after B doping, both the (100) peak intensity and the grain size of the BZO film had notably decreased. After annealing at 450 °C and Se doping, the (110) peak intensity and grain size of the ZnOSe/ZnO/BZO multi-layer increased, but remained smaller than those of the pristine ZnO photoanode. The smaller grain size correlated with an increase in light absorption (Figure S3, Supporting Information). Notably, the (110) peak of the ZnOSe/ZnO/BZO photoanode shifted towards a lower diffraction angle because the ionic radius of Se^{2-} is larger than that of O^{2-}.[25] This result suggests that the Se atoms have been incorporated into the ZnO crystal lattices.

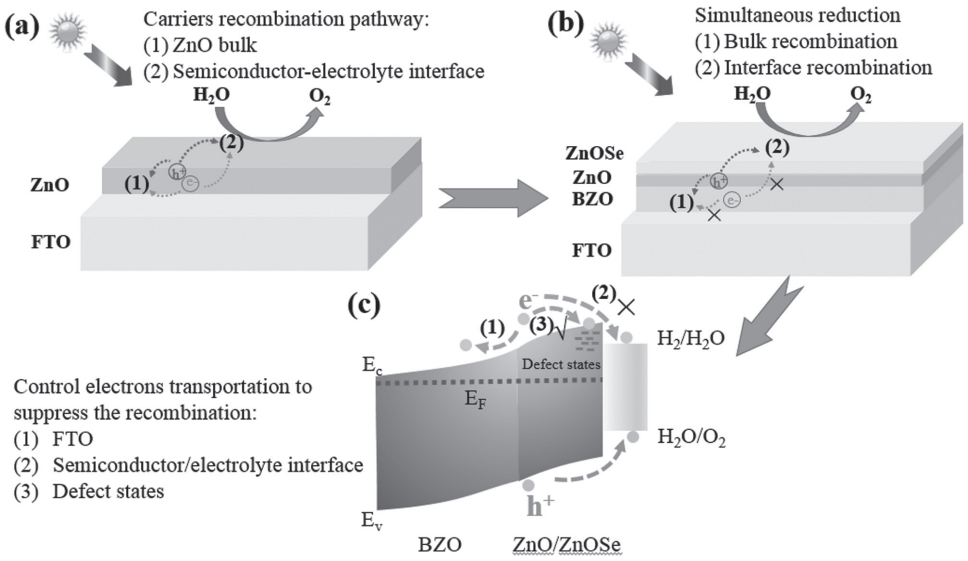

Figure 1. a) Schematic illustration of two main electron–hole recombination pathways in ZnO photoanode for PEC water splitting, b) the proposed ZnOSe/ZnO/BZO multi-layer structure to reduce bulk and interfacial recombination, and c) photo-induced electron–hole transfer processes in ZnOSe/ZnO/BZO structure.

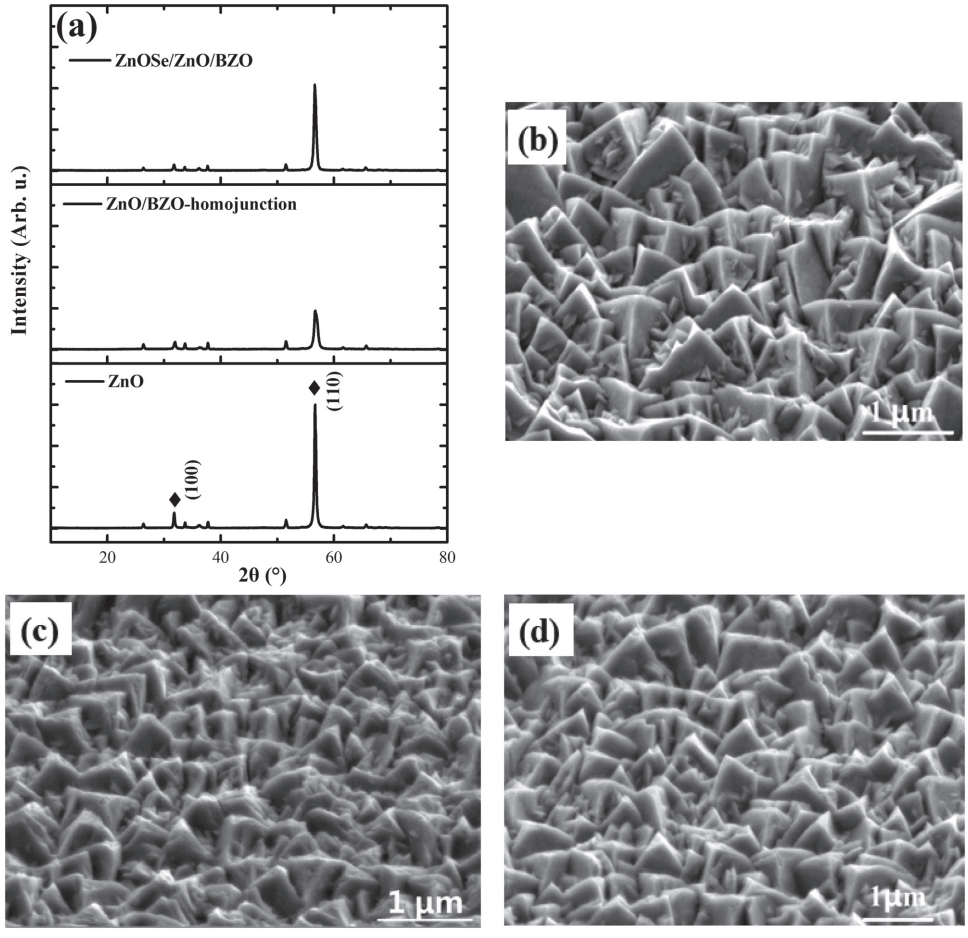

Figure 2. a) XRD patterns of the anodes used in this work. b–d) SEM images of ZnO (b), ZnO/BZO-homojunction (c), and ZnOSe/ZnO/BZO photoanodes (d).

X-ray photoelectron spectroscopy (XPS) was used to further check whether the Se atoms had been incorporated into the ZnO lattices. The XPS spectra (Figure S2, Supporting Information) revealed that all Zn, O, and Se signals appeared in the Se-doped ZnO photoanode. In the Se 3d core-level spectra of the samples (**Figure 3**a), the peak for ZnOSe was located at 52.6 eV, which was lower than that in previous reports, ≈55 eV.[26,27] This decrease in the binding energy may be due to a partial replacement of O by Se in ZnOSe.[28] In the Zn 2p core-level spectra, the Zn $2p_{3/2}$ peak for ZnOSe was located at around 1020 eV, which was lower than that of ZnO (1020.4 eV) (Figure 3b).[29] These results indicate that Se has been successfully incorporated into the ZnO lattice and has formed Zn-Se bonds.

To determine the Se concentration and distribution with depth, we carried out secondary ion mass spectrometry (SIMS) (Figure 3c). As expected, the concentration of Se decreased with the depth. Se can react with O to form SeO_2 and sublime at around 315 °C, leading to the observed sharp decrease in its concentration near the top surface and another sub-peak at 300-nm depth.

We further carried out ultraviolet photoelectron spectrometry (UPS, **Figure 4**) to examine the work functions of the BZO and ZnO thin films. The UPS results suggest that B incorporation does not affect the Fermi edge position (being distinct from the Fermi level, which is determined by the Fermi edge position and the cutoff edge position). The low energy cutoff edge does shift to a lower energy position compared to pristine ZnO. The work function can be determined as follows:

$$\Phi = h\nu + E_{\text{Cutoff}} - E_{\text{Fermi}} \tag{1}$$

where $h\nu$ is the excitation source energy, and E_{Cutoff} and E_{Fermi} are the cutoff edge energy and Fermi edge energy, respectively. These findings indicate that the work function of BZO is lower than that of pristine ZnO. As indicated in Figure 1c, band-bending and the built-in electric field in the BZO/ZnO structure facilitate the separation and transport of photo-generated charge carriers,[30–32] which helps to reduce the charge recombination in the bulk.

An electric field in a photoanode can be generated by a spatial variation of the Fermi level — a possibility that can readily be monitored by investigating the carrier concentration. We therefore used Hall-effect measurements to determine the carrier concentrations in the BZO and ZnO thin films. The results showed carrier concentrations of 1.0×10^{20} and 1.4×10^{19} cm^{-3} in BZO and ZnO, respectively. The Fermi level in BZO was shifted upwards compared to ZnO according to[33]

$$\Delta E = E_{\text{F,BZO}} - E_{\text{F,ZnO}} = kT \ln\left(\frac{N_{\text{D,BZO}}}{N_{\text{D,ZnO}}}\right) \tag{2}$$

where k is the Boltzmann constant, T is the temperature in Kelvin, and $N_{\text{D,BZO}}$ and $N_{\text{D,ZnO}}$ are the carrier concentrations

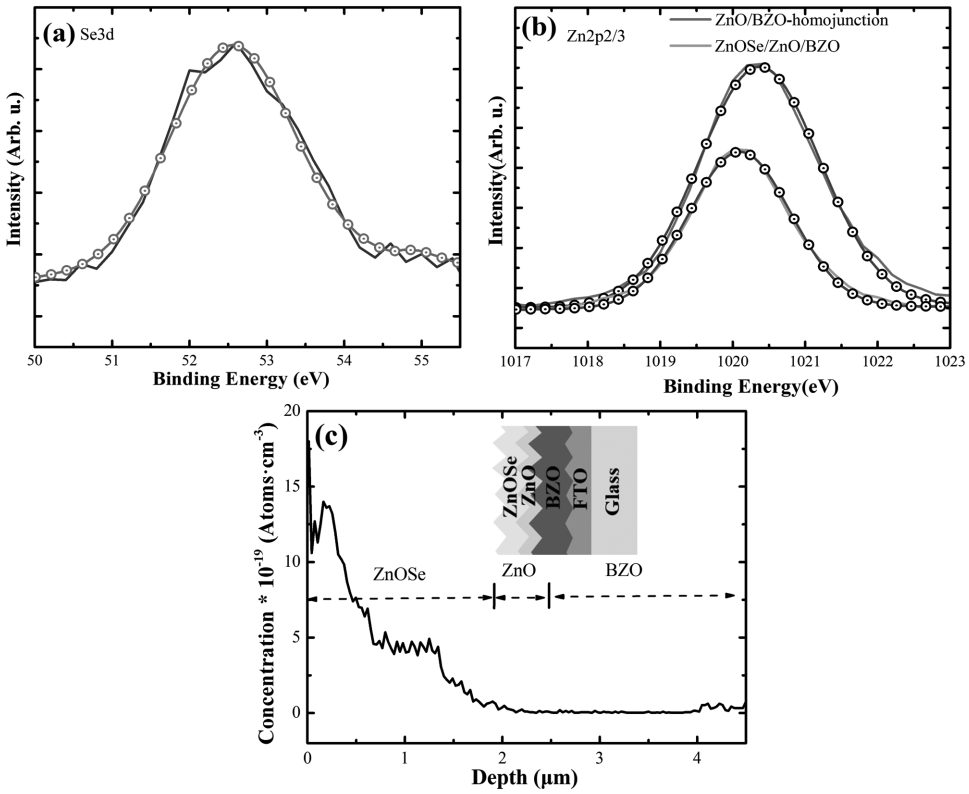

Figure 3. a) Se 3d XPS fitting results of ZnOSe/ZnO/BZO thin-film photoanode; b) Zn $2p_{2/3}$ XPS fitting results of ZnO/BZO homojunction (upper line) and ZnOSe/ZnO/BZO thin film photoanode (lower line), and c) the SIMS results of the Se concentration in ZnOSe/ZnO/BZO photoanode, the inset is a sketch of the structure of the photoanode.

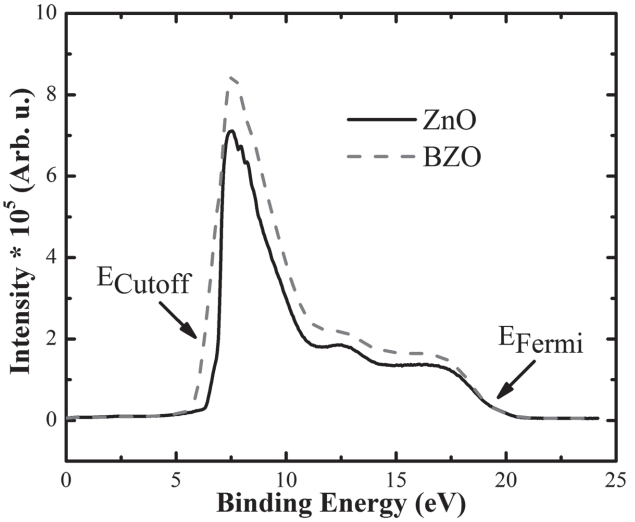

Figure 4. The UPS testing curves for BZO and ZnO thin films.

of the BZO and ZnO thin films, respectively. Thus BZO combined with ZnO provides an n^+–n homojunction that can facilitate electron transport and impede bulk recombination.

To reduce the charge accumulation at the solid–liquid interface, we introduced oxygen vacancies at the ZnO/BZO-homojunction via doping using Se. Under a high thermal evaporation temperature, the Se atoms replace the O atoms in a ZnO lattice and induce a lattice distortion in the ZnO, resulting in increased vacancies. The XPS data (**Figure 5**) shows that the prominent O 1s peak at ≈528 eV corresponds to the Zn-O bonds, whereas the shoulder at ≈530 eV can be assigned to the oxygen vacancies.[34] For Se-doped photoanodes, the oxygen atomic ratio in the films was reduced from an initial 60% to 51%. The corresponding absorption spectra of ZnOSe/ZnO/BZO thin-film photoanodes exhibited high visible-light absorption (Figure S3, Supporting Information), which could be caused by the existence of oxygen vacancies in the ZnO bandgap.[35] Oxygen vacancies in metal oxides can act as electron donors,[36] which will tend to increase the carrier concentration in the conduction band and produce a blue shift in the absorption band-edge (Figure S3b).[37,38]

The Mott–Schottky (M–S) method was used to investigate the electrical properties of the photoanodes. According to the M–S equations:[39,40]

$$1/C^2 = \left(2/e_0\varepsilon\varepsilon_0\right)\left((V - V_{FB}) - kT/e_0\right) \quad (3)$$

$$N_d = \left(2/e_0\varepsilon\varepsilon_0\right)\left(d\left(1/C^2\right)/dV\right)^{-1} \quad (4)$$

where e_0 is the electric charge, ε is the dielectric constant of ZnO, ε_0 is the permittivity of vacuum, N_d is the doped density, V is the electrode applied potential, V_{FB} is the flat-band potential, and kT/e_0 is a temperature-dependent correction term. The M–S plots collected from the ZnO, ZnO/BZO, and ZnOSe/ZnO/BZO photoanodes are presented in **Figure 6**a. The results show that N_d increased from an initial 7.1×10^{19} to 4.1×10^{21} and 1.5×10^{22} cm^{-3}. We associated this with the doping of B atoms and the generation of oxygen vacancies by Se-doping. The V_{FB} shifted from an initial –0.56 V to –0.71 V and –0.75 V, resulting in an upward-shift of the Fermi level and corresponding band-bending. The ZnOSe/ZnO/BZO photoanode had a larger V_{FB} than that of the ZnO/BZO-homojunction photoanode, which was consistent with a Fermi level upward shift induced by the incorporation of Se atoms. As the V_{FB} position will affect the position of its flat-band potential, we amplified the range of –0.3–0.3 V vs. Ag/AgCl of **Figure 7**a to observe the onset potential of the samples. It can clearly be seen that the ZnOSe/ZnO/BZO photoanode has the lowest onset potential, as is shown in Figure S4 (Supporting Information).

Figure 6b shows the Nyquist plots for the photoanodes in the dark at 0.62 V versus Ag/AgCl.[41,42] We obtained these using potentiostatic electrochemical impedance spectroscopy. Using the equivalent circuit models shown in the inset, we obtained the equivalent series resistance (R_s); bulk material resistance (R_{bulk}), charge-transfer resistance (R_{ct}), space charge region capacitance (CPE2), and the Helmholtz capacitance (CPE1). The R_{ct} of the ZnO/BZO photoanode had decreased compared to that of the ZnO photoanode (655 KΩ→260 KΩ), which is consistent with the formation of a built-in electric field. The lower R_{ct} illustrates that the homojunction structure favors carrier transport in the bulk. Notably, ZnOSe/ZnO/BZO has a smaller R_{ct} than both the ZnO/BZO-homojunction and ZnO photoanodes, confirming that the ZnOSe/ZnO/BZO structure helps to separate photogenerated electron–hole pairs.

To investigate the activities of the aforementioned structures, we studied the PEC performances of the ZnO, ZnO/BZO, and ZnOSe/ZnO/BZO photoanodes. The photocurrent curves were obtained under simulated sunlight (100 mW cm^{-2}) illumination (Figure 7a). The photocurrent density measured at 0.62 V (vs. Ag/AgCl) for the ZnO/BZO homojunction (ca. 0.4 mA cm^{-2}) was 1.3 times higher than that of pristine ZnO. To further investigate the improvement in PEC performance using the homojunction structure, a homogeneous BZO thin film photoanode (h-BZO) and a reversed ZnO/BZO homojunction (r-ZnO/BZO homojunction, BZO layer contacting with electrolyte) were

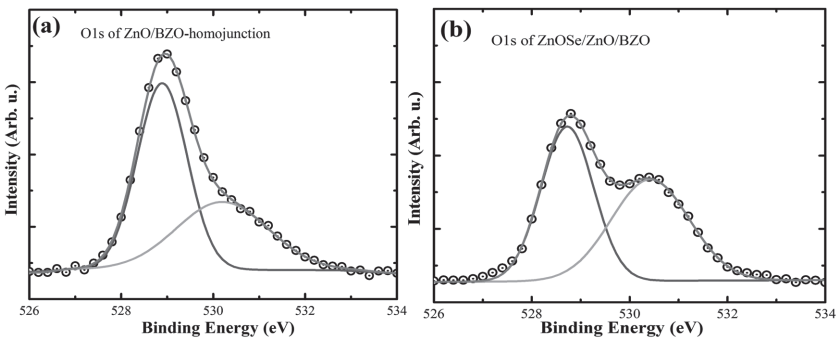

Figure 5. a,b) O 1s XPS spectra of ZnO (a) and ZnOSe (b) in the ZnO/BZO homojunction and ZnOSe/ZnO/BZO thin-film photoanodes, respectively.

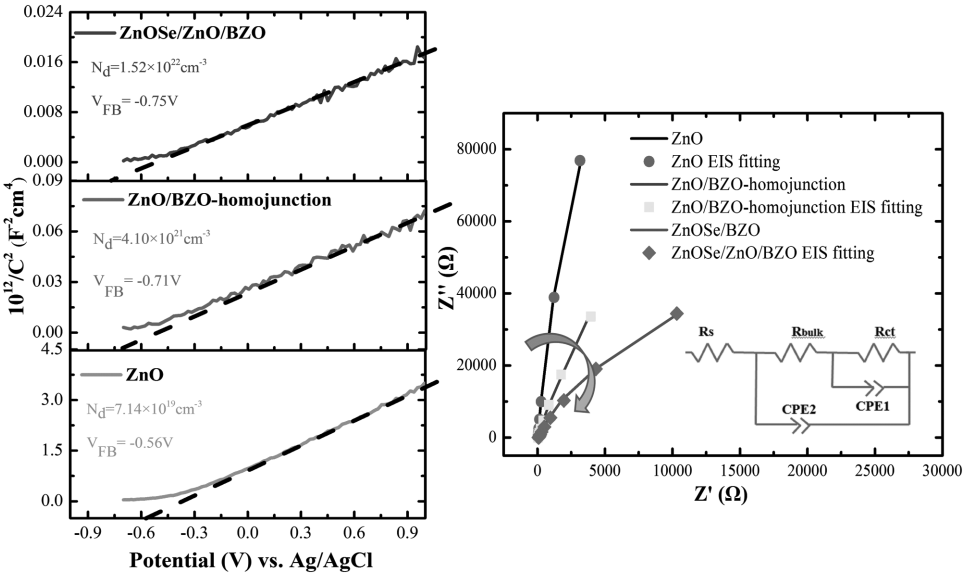

Figure 6. a) Mott–Schottky plots of ZnO, ZnO/BZO-homojunction, and ZnOSe/ZnO/BZO measured in the dark at a frequency of 5 kHz and an AC current of 10 mV with a three-electrode system. b) Nyquist plots of ZnO, ZnO/BZO-homojunction, and ZnOSe/ZnO/BZO photoanodes in the dark at 0.62 V vs. Ag/AgCl in 0.5 M Na_2SO_4 aqueous solution. The inset shows the equivalent circuits.

prepared. The photocurrent of both structures decreased significantly, and even remained below that of the undoped ZnO anode. These results confirm the better charge separation in the ZnO/BZO homojunction. The ZnOSe/ZnO/BZO photoanode showed an impressive increase in current density, which reached 1.1 mA cm^{-2} at 0.62 V (vs. Ag/AgCl). We attribute the increased photocurrent density to the combination of the beneficial effects of both the homojunction structure and the oxygen vacancies of the ZnOSe layer.

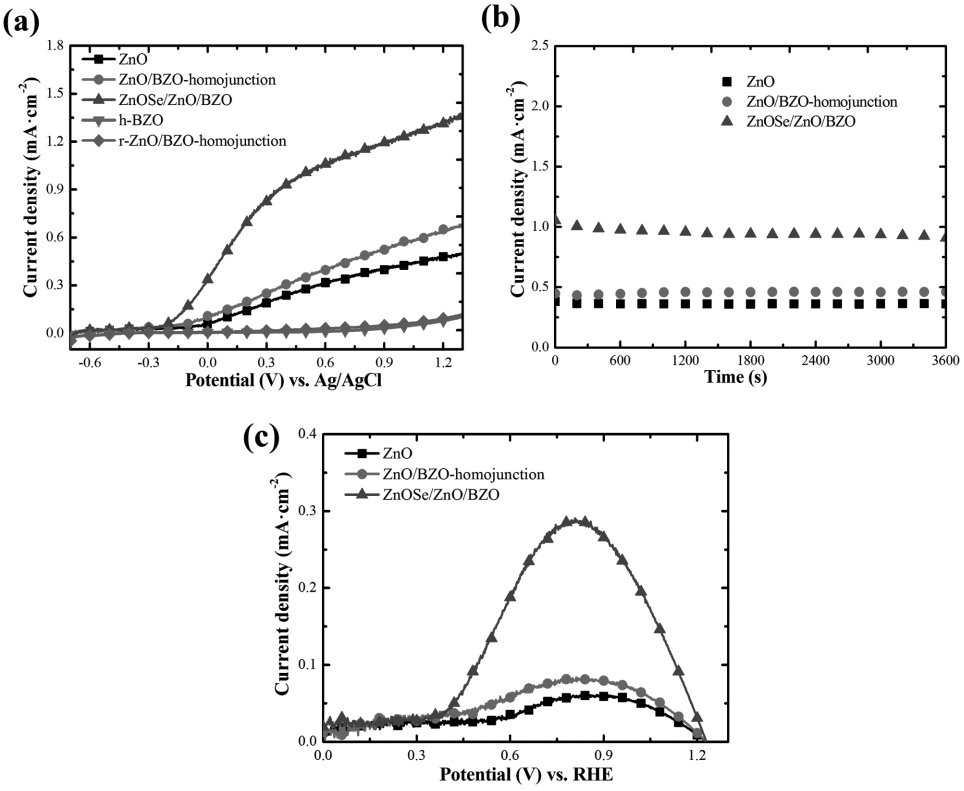

Figure 7. Photoelectrochemical properties: a) Linear-sweep voltammetry curves of ZnO, ZnO/BZO-homojunction, ZnOSe/ZnO/BZO, t-BZO, and r-ZnO/BZO-homojunction photoanodes. b) Photocurrent retention performance of ZnO, ZnO/BZO-homojunction, and ZnOSe/ZnO/BZO at an applied voltage of 0.62 V vs. Ag/AgCl under illumination. c) Photocurrent conversion efficiency (PCE) curves for ZnO, ZnO/BZO-homojunction, and ZnOSe/ZnO/BZO anodes.

Table 1. Process parameters of ZnO, ZnO/BZO-homojunction, and ZnOSe/ZnO/BZO.

Sample No.	First layer	Second layer	ZnOSe layer thickness (μm)
	BZO layer doping flow/thickness (sccm/μm)	ZnO layer thickness (μm)	
ZnO	–	5	–
ZnO/BZO-homojunction	7/1.5	2.5	–
ZnOSe/ZnO/BZO	7/1.5	0.5	2

The PEC stability of ZnO, ZnO/BZO, and ZnOSe/ZnO/BZO under 100 mW cm^{-2} illumination at 0.62 V vs. Ag/AgCl was measured using an amperometric *I–t* study (Figure 7b). All photoanodes exhibited a good stability for PEC water splitting. The high photocurrent conversion efficiency (PCE) of the ZnOSe/ZnO/BZO anode (0.3%), which was five times higher than that of pristine ZnO (0.06%) (Figure 7c), confirmed the suppression of charge recombination via the joint bulk and interfacial benefits.

Table S1 (Supporting Information) lists the PEC performance of the various ZnO photoanodes explored herein. We found that the PEC performance of the ZnOSe/ZnO/BZO structure was superior to that reported for ZnO thin-film photoanodes. This high PEC performance indicates the great promise of the ZnOSe/ZnO/BZO structure for solar-driven water-splitting systems.

In conclusion, this work reports a significant enhancement in the photocurrent of ZnO-based photoanodes for solar water splitting. It is achieved via a design that combines an n^+–n homojunction with an oxygen-vacancy-rich surface. The built-in electric field in the ZnO/BZO homojunction impeded bulk charge recombination and accelerated photo-generated charge-carrier transport. The ZnOSe/ZnO/BZO structure, with its oxygen vacancies at the surface of the photoanode, inhibited the surface recombination at the photoanode/electrolyte interface and also contributed to enhanced charge transport. The catalyst-free ZnOSe/ZnO/BZO photoanode increased the photocurrent density to 1.12 mA cm^{-2} at 0.62 V vs. Ag/AgCl (1.23 V vs. RHE). To the best of our knowledge this is the best performance reported so far among currently known ZnO photoanodes. The combination of a n–n^+ homojunction structure and surface doping suggests a path for related metal oxide photoanodes to improve their PEC performance.

Experimental Section

Photoanode Fabrication: ZnO thin-film photoanodes were deposited on fluorine-doped tin oxide (FTO) substrates using low-pressure chemical vapor deposition (LPCVD). Diethylzinc (DEZn) and water vapor were directly evaporated into the system as the precursors. The DEZn and H_2O flow rates were set at 180 and 110 sccm, respectively. The total pressure was 75 Pa inside the reactor, and the growth temperature was 155 °C. Se atoms were introduced onto the ZnO film via thermal evaporation to prepare ZnOSe/ZnO/BZO photoanodes. The thermal evaporation temperature and reaction time were 450 °C and 45 min, respectively. The processing parameters of the ZnO, ZnO/BZO-homojunction, and ZnOSe/ZnO/BZO structure are listed in **Table 1**.

Material Characterizations: We characterized the ZnO thin-film photoanodes using X-ray diffraction (XRD, Rigaku-Dmax-2500, λ = 1.54806 Å for Cu Kα) in the range of 10–80°. Scanning electron microscopy (SEM, Zeiss-Supra 550p) was used to monitor the variations in surface morphology of the deposited samples. Optical absorption of the samples was measured in the wavelength range of 300–600 nm using a UV–vis–NIR spectrophotometer (Varian-Cary 5000). The work function was analyzed using ultraviolet photoelectron spectroscopy (UPS, Thermo WSCALAB 250). The Se concentration was characterized using secondary ion mass spectrometry (SIMS, Cameca 4F). The chemical state of the photoanodes was investigated using X-ray photoelectron spectroscopy (XPS, Thermo WSCALAB 250). All measurements were carried out at room temperature.

PEC Performance Characterization: All PEC measurements were carried out on an electrochemical workstation (PARSTAT 4000, Princeton Applied Research, USA) using a home-built three-electrode optical cell using Ag/AgCl as the reference electrode and a Pt wire as the counter electrode. The as-prepared ZnO-based photoanodes were used as the working electrode with a testing area of 0.283 cm^2. A Na_2SO_4 aqueous solution (0.5 M) with a pH of 7.0 was used as the electrolyte. The ZnO thin-film photoanode was illuminated under AM 1.5G simulated solar light with a light intensity of 100 mW cm^{-2}. Linear sweep voltammetry (LSV) was acquired using an electrochemical workstation in the voltage range of –0.7 to 1.3 V vs. Ag/AgCl and the scanning rate was 10 mV s^{-1}. Amperometric *I–t* curves of the ZnO thin-film photoanodes were obtained at an applied voltage of 0.62 V vs. Ag/AgCl (1.23 V vs. the reversible hydrogen electrode (RHE)) at 100 mW cm^{-2}. Nyquist plots were acquired in the dark at 0.62 V vs. Ag/AgCl in 0.5 M Na_2SO_4 aqueous solution.

Supporting Information

Supporting Information is available from the Wiley Online Library or from the author.

Acknowledgements

The authors gratefully acknowledge the support from the International cooperation projects of the Ministry of Science and Technology (2014DFE60170), the National Natural Science Foundation of China (Grant No. 61474065), the Tianjin Research Key Program of Application Foundation and Advanced Technology (15JCZDJC31300), the Key Project in the Science & Technology Pillar Program of Jiangsu Province (BE2014147-3), and the 111 Project (B16027). H.T. acknowledges the Dutch Organisation for Scientific Research (NWO) for a Rubicon grant (680-50-1511) to support his postdoctoral research at the University of Toronto.

[1] O. Khaselev, J. A. Turner, *Science* **1998**, *280*, 425.
[2] R. E. Blankenship, D. M. Tiede, J. Barber, G. W. Brudvig, G. Fleming, M. Ghirardi, M. R. Gunner, W. Junge, D. M. Kramer, A. Melis, T. A. Moore, C. C. Moser, D. G. Nocera, A. J. Nozik, D. R. Ort, W. W. Parson, R. C. Prince, R. T. Sayre, *Science* **2011**, *332*, 805.
[3] S. D. Tilley, M. Schreier, J. Azevedo, M. Stefik, M. Graetzel, *Adv. Funct. Mater.* **2014**, *24*, 303.
[4] A. Azarpira, M. Lublow, A. Steigert, P. Bogdanoff, D. Greiner, C. A. Kaufmann, M. Krüger, U. Gernert, R. Van De Krol, A. Fischer, T. Schedel-Niedrig, *Adv. Energy Mater.* **2015**, *5*, 1402148.
[5] C. L. Zhang, M. F. Shao, F. Y. Ning, S. M. Xu, Z. H. Li, M. Wei, D. G. Evans, X. Duan, *Nano Energy* **2015**, *12*, 231.
[6] S. Xie, X. Lu, T. Zhai, W. Li, M. Yu, C. Liang, Y. Tong, *J. Mater. Chem.* **2012**, *22*, 14272.
[7] Y. G. Lin, Y. K. Hsu, Y. C. Chen, S. B. Wang, J. T. Miller, L. C. Chen, K. H. Chen, *Energy Environ. Sci.* **2012**, *5*, 8917.
[8] A. Wolcott, W. A. Smith, T. R. Kuykendall, Y. Zhao, J. Z. Zhang, *Adv. Funct. Mater.* **2009**, *19*, 1849.
[9] A. M. Pawar, C. W. Kim, M. J. Kang, Y. S. Kang, *Nano Energy* **2016**, *20*, 156.
[10] Y. Li, X. Zhang, S. Jiang, H. Dai, X. Sun, Y. Li, *Sol. Energy Mater. Sol. Cells* **2015**, *132*, 40.
[11] K. J. Feng, W. Li, S. L. Xie, X. H. Lu, *Electrochim. Acta* **2014**, *137*, 108.
[12] X. Y. Yang, A. Wolcott, G. M. Wang, A. Sobo, R. C. Fitzmorris, F. Qian, J. Z. Zhang, Y. Li, *Nano Lett.* **2009**, *9*, 2331.
[13] C. Jiang, S. J. A. Moniz, M. Khraisheh, J. Tang, *Chem. Eur. J.* **2014**, *20*, 12954.
[14] Y. K. Hsu, Y. C. Chen, Y. G. Lin, *ACS Appl. Mater. Interfaces* **2015**, *7*, 14157.
[15] S. J. A. Moniz, J. Zhu, J. Tang, *Adv. Energy Mater.* **2014**, *4*, 1301590.
[16] B. S. Shaheen, H. G. Salem, M. A. El-Sayed, N. K. Allam, *J. Phys. Chem. C* **2013**, *117*, 18502.
[17] Q. Li, X. Sun, K. Lozano, Y. Mao, *J. Phys. Chem. C* **2014**, *118*, 13467.
[18] Y. Qiu, K. Yan, H. Deng, S. Yang, *Nano Lett.* **2012**, *12*, 407.
[19] M. Shao, F. Ning, M. Wei, D. G. Evans, X. Duan, *Adv. Funct. Mater.* **2014**, *24*, 580.
[20] M. Eron, A. Rothwarf, *J. Appl. Phys.* **1985**, *57*, 2275.
[21] M. Saad, A. Kassis, *Sol. Energy Mater. Sol. Cells* **2003**, *79*, 507.
[22] F. F. Abdi, L. Han, A. H. Smets, M. Zeman, B. Dam, R. V. D. Krol, *Nat. Commun.* **2013**, *4*, 2195.
[23] M. K. Nowotny, L. R. Sheppard, T. Bak, J. Nowotny, *J. Phys. Chem. C* **2008**, *112*, 5275.
[24] M. A. Rahman, S. Bazargan, S. Srivastava, X. Wang, M. Abd-Ellah, J. P. Thomas, N. F. Heinig, D. Pradhan, K. T. Leung, *Energy Environ. Sci.* **2015**, *8*, 3363.
[25] G. Y. Lan, Y. W. Lin, Y. F. Huang, H. T. Chang, *J. Mater. Chem.* **2007**, *17*, 2661.
[26] B. P. Nenavathu, A. V. R. Krishna Rao, A. Goyal, A. Kapoor, R. K. Dutta, *Appl. Catal. A* **2013**, *459*, 106.
[27] A. M. Chaparro, C. Maffiotte, M. T. Gutierrez, J. Herrero, *Thin Solid Films* **2000**, *358*, 22.
[28] H. Cai, H. Xu, H. Z. Ye, J. Huang, *Mater. Lett.* **2013**, *108*, 183.
[29] W. Niu, H. Xu, Y. Guo, Y. Li, Z. Ye, L. Zhu, *Phys. Chem. Chem. Phys.* **2015**, *17*, 16705.
[30] S. K. Pilli, T. G. Deutsch, T. E. Furtak, L. D. Brown, J. A. Turner, A. M. Herring, *Phys. Chem. Chem. Phys.* **2013**, *15*, 3273.
[31] S. J. Hong, S. Lee, J. S. Jang, J. S. Lee, *Energy Environ. Sci.* **2011**, *4*, 1781.
[32] S. Hernandez, V. Cauda, A. Chiodoni, S. Dallorto, A. Sacco, D. Hidalgo, E. Celasco, C. F. Pirri, *ACS Appl. Mater. Interfaces* **2014**, *6*, 12153.
[33] W. A. Smith, I. D. Sharp, N. C. Strandwitz, J. Bisquert, *Energy Environ. Sci.* **2015**, *8*, 2851.
[34] C. Hu, K. Chu, Y. Zhao, W. Y. Teoh, *ACS Appl. Mater. Interfaces* **2014**, *6*, 18558.
[35] B. Sambandam, R. J. Michael, P. T. Manoharan, *Nanoscale* **2015**, *7*, 13935.
[36] K. M. Wong, Y. Fang, A. Devaux, L. Wen, J. Huang, L. De Cola, Y. Lei, *Nanoscale* **2011**, *3*, 4830.
[37] B. K. Meyer, A. Polity, B. Farangies, Y. He, D. Hasselkamp, T. Krämer, C. Wang, *Appl. Phys. Lett.* **2004**, *85*, 4929.
[38] K. J. Kim, Y. R. Park, *Appl. Phys. Lett.* **2001**, *78*, 475.
[39] S. Ho-Kimura, S. J. A. Moniz, A. D. Handoko, J. Tang, *J. Mater. Chem. A* **2014**, *2*, 3948.
[40] M. Radecka, M. Rekas, A. Trenczek-Zajac, K. Zakrzewska, *J. Power Sources* **2008**, *181*, 46.
[41] A. A. Dubale, C. J. Pan, A. G. Tamirat, H. M. Chen, W. N. Su, C. H. Chen, J. Rick, D. W. Ayele, B. A. Aragaw, J. F. Lee, Y. W. Yang, B. J. Hwang, *J. Mater. Chem. A* **2015**, *3*, 12482.
[42] L. Zhang, E. Reisner, J. J. Baumberg, *Energy Environ. Sci.* **2014**, *7*, 1402.

Received: October 20, 2016
Revised: November 24, 2016
Published online: January 5, 2017

